Inorg. Chem. **2007**, *46*, 6968–6979

High-Spin Mn Wheels

Maria Manoli,[†] Alessandro Prescimone,[†] Rashmi Bagai,[‡] Abhudaya Mishra,[‡] Muralee Murugesu,[‡] Simon Parsons,[†] Wolfgang Wernsdorfer,[§] George Christou,[‡] and Euan K. Brechin*,[†]

School of Chemistry, The University of Edinburgh, West Mains Road, Edinburgh EH9 3JJ, U.K., Department of Chemistry, University of Florida, Gainesville, Florida 32611-7200, and Laboratoire Louis Néel-CNRS, 38042 Grenoble, Cedex 9, France

Received April 20, 2007

The syntheses, structures, and magnetic properties of the complexes $[Mn^{IV}_4Mn^{III}_{10}Mn^{II}_2O_2(OCH_3)_{12}(tmp)_8(O_2CCH_3)_{10}]\cdot 3Et_2O$ (**1**·$3Et_2O$), $[Mn^{IV}_2Mn^{III}_{18}Mn^{II}_2O_6(OCH_3)_{14}(O_2CCH_3)_{16}(tmp)_8(HIm)_2]\cdot 2CH_3OH$ (**2**·$2CH_3OH$), and $[Mn^{IV}_2Mn^{III}_{18}Mn^{II}_2O_6(OCH_3)_{14}(O_2CCH_3)_{16}(Br{-}mp)_8(HIm)_2]\cdot 2C_6H_{14}\cdot 5CH_3OH$ (**3**·$2C_6H_{14}$·$5CH_3OH$) are reported. The unusual wheel-like complexes were prepared by the treatment of $[Mn_3O(O_2CCH_3)_6(HIm)_3](O_2CCH_3)$ (HIm = imidazole) with 1,1,1-tris(hydroxymethyl)propane (H_3tmp) (**1** and **2**) or 2-(bromomethyl)-2-(hydroxymethyl)-1,3-propanediol ($Br{-}mpH_3$) (**3**) in the presence of sodium methoxide ($NaOCH_3$, **2**, and **3)** in CH_3OH. Complex **1**·$3Et_2O$ crystallizes in the triclinic space group $P\bar{1}$, while complexes **2**·$2CH_3OH$ and **3**·$2C_6H_{14}$·$5CH_3OH$ crystallize in the orthorhombic space group *Pbca*. Direct current magnetic susceptibility data, collected for **1**–**3** in the respective 1.8–300 K and 0.1–7 T temperature and magnetic-field ranges, afford spin ground-state values of $S = 14 \pm 1$ for complex **1** and $S = 9 \pm 1$ for complexes **2** and **3**. Alternating current susceptibility measurements performed on all three complexes in the 1.8–10 K temperature range in a 3.5 G oscillating field at frequencies between 50 and 1000 Hz reveal out-of-phase χ''_M signals below approximately 3 K. Single-crystal hysteresis loop and relaxation measurements confirm single-molecule magnetism behavior.

Introduction

The synthesis of polynuclear manganese clusters constitutes an important modern facet of chemistry and physics, with the advent of single-molecule magnetism a catalyst for the resurgence of worldwide interest.[1] Single-molecule magnets (SMMs) are molecules that display magnetization hysteresis that is purely intramolecular in origin and as such potentially represent a technologically important family of complexes. Many polynuclear clusters containing 3d transition metals have since been reported to be SMMs despite the relative difficulty in obtaining molecules that contain relatively high spin ground-state values in combination with Ising-type anisotropy.[2] Isotropic high-spin polynuclear clusters cannot function as nanoscale magnets but are candidates to act as very low-temperature magnetic refrigerants.[3] The vast majority of SMMs contain manganese and are mixed-valent clusters containing multiple Mn^{III} ions whose Jahn−

Chart 1. Structures of 1,1,1-tris(hydroxymethyl)propane (H_3tmp) and 2-(bromomethyl)-2-(hydroxymethyl)-1,3-propanediol ($Br{-}mpH_3$)

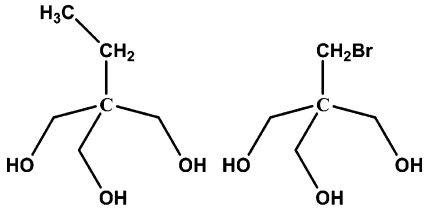

H_3tmp **$Br\text{-}mpH_3$**

* To whom correspondence should be addressed. E-mail: ebrechin@staffmail.ed.ac.uk.
[†] University of Edinburgh.
[‡] University of Florida.
[§] Laboratoire Louis Néel.

(1) (a) Sessoli, R.; Tsai, H.-L.; Schake, A. R.; Wang, S. Y.; Vincent, J. B.; Folting, K.; Gatteschi, D.; Christou, G.; Hendrickson, D. N. *J. Am. Chem. Soc.* **1993**, *115*, 1804. (b) Sessoli, R.; Gatteschi, D.; Caneschi, A.; Novak, M. A. *Nature* **1993**, *365*, 141. (c) Gatteschi, D.; Sessoli, R. *Angew. Chem., Int. Ed.* **2003**, *42*, 268. (d) Caneschi, A.; Gatteschi, D.; Sessoli, R.; Barra, A. L.; Brunel, L. C.; Guillot, M. *J. Am. Chem. Soc.* **1991**, *113*, 5873.

(2) Aromí, G.; Brechin, E. K. *Struct. Bonding (Berlin, Ger.)* **2006**, *122*, 1.

(3) (a) Evangelisti, M.; Luis, F.; Jongh, L. J.; Affronte, M. *J. Mater. Chem.* **2006**, *16*, 2534. (b) Evangelisti, M.; Candini, A.; Ghirri, A.; Affronte, M.; Brechin, E. K.; McInnes, E. J. L. *Appl. Phys. Lett.* **2005**, *87*, 072504.

10.1021/ic7007528 CCC: $37.00
Published on Web 07/21/2007

Scheme 1. Bonding Modes Employed by a Variety of Ligands for the Assembly of Mn Wheels

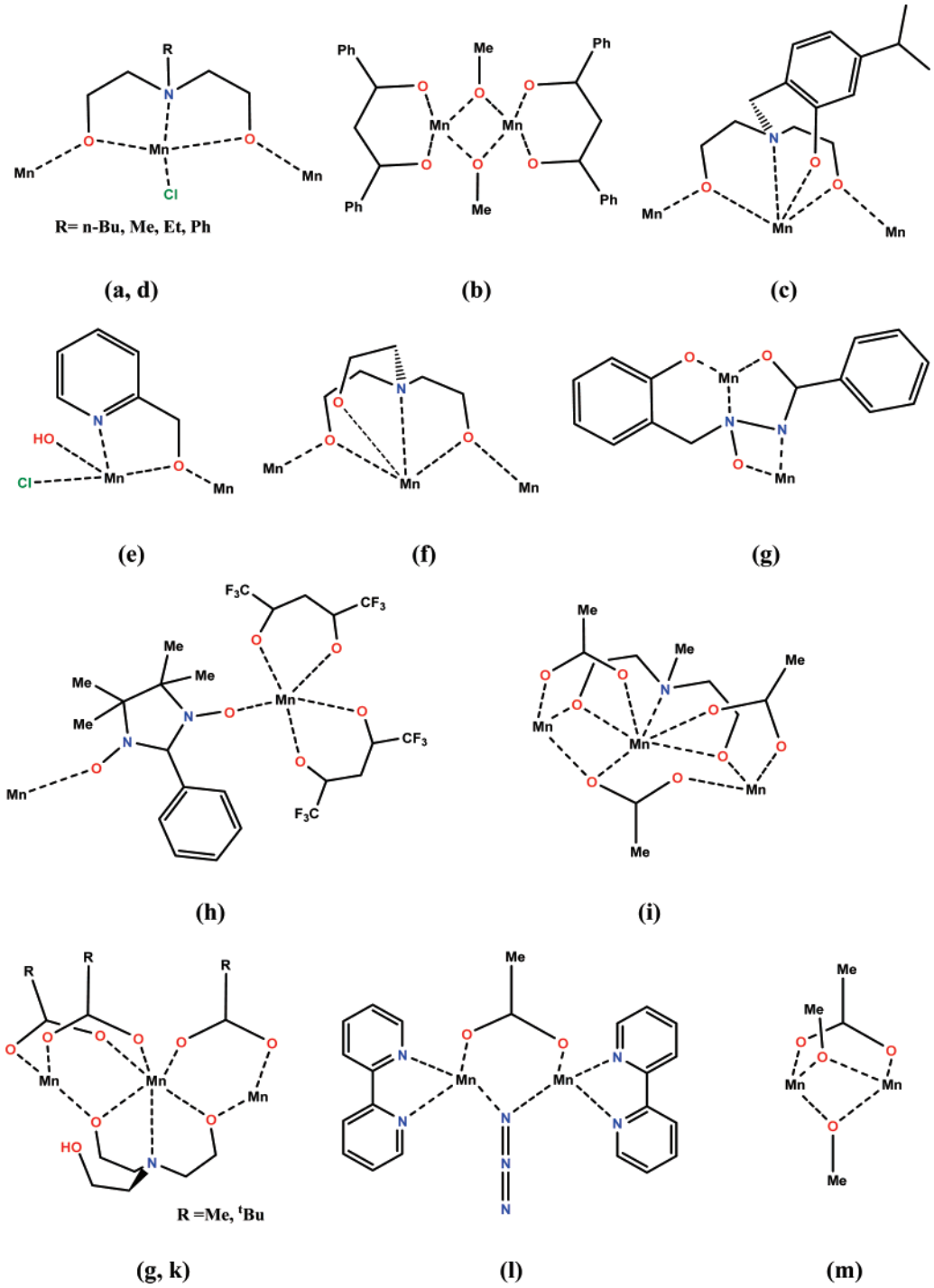

Teller axes are co-parallel.[4] They vary in nuclearity from 2 to 84 and form a plethora of aesthetically pleasing topologies ranging from simple dimers, triangles, and cubes to discs, icosahedra, and wheels.[1,2,4,5] This latter class of complexes is extremely rare in Mn^{III} chemistry despite being rather common for Fe^{III}, Ga^{III}, Cr^{III}, and V^{III},[6−9] though there are reports of isostructural Fe and Mn clusters, for example, $[Mn^{III}(C_{14}H_9N_2O_3)(CH_3OH)]_{10}$ and $[Fe^{III}(C_{14}H_9N_2O_3)(CH_3OH)]_{10}$.[8a] The nuclearity of Mn wheels varies from 6 to 84 and can be divided into 3 main categories. The first describes metal-centered complexes or "metallocycles",[7a−g] with the most common being the heptanuclear $\{Mn^{II}[Mn^{II}_2Mn^{III}_4]\}$ clusters (neutral, anionic, or cationic), examples of which include $\{Mn^{II}[Mn^{II}_2Mn^{III}_4Cl_6(L^3)_6]\}$ (L = *N*-*n*-butyldiethanolamine) (**a**), $\{Mn^{II}[Mn^{II}_2Mn^{III}_4(OCH_3)_{12}(dbm)_6]\}$ (Hdbm = dibenzoyldimethane) (**b**), $\{Mn^{II}[Mn^{II}_2Mn^{III}_4Cl_6(L^4)_6]\}$ (H_3L^4 = *N*-(2-hydroxy-5-nitrobenzyl)iminodiethanol) (**c**),

(4) (a) Gatteschi, D.; Sessoli, R. *Angew. Chem., Int. Ed.* **2003**, *42*, 268. (b) Bircher, R.; Chaboussant, G.; Dobe, C.; Güdel, H. U.; Ochsenbein, S. T.; Sieber, A.; Waldman, O. *Adv. Funct. Mater.* **2006**, *16*, 209. (c) Christou, G. *Polyhedron* **2005**, *24*, 2065. (d) Brechin, E. K. *Chem. Commun.* **2005**, 5141. (e) Hendrickson, D. N.; Christou, G.; Ishimoto, H.; Yoo, J.; Brechin, E. K.; Yamaguchi, A. E.; Rumberger, M.; Aubin, S. M. J.; Sun, Z.; Aromí, G. *Mol. Cryst. Liq. Cryst.* **2002**, *376*, 301.

Table 1. Crystallographic Data for Complexes **1**·3Et_2O, **2**·2CH_3OH, and **3**·2C_6H_{14}·5CH_3OH

	1·3Et_2O	**2**·2CH_3OH	**3**·2C_6H_{14}·5CH_3OH
formula[a]	$C_{92}H_{184}Mn_{16}O_{61}$	$C_{102}H_{192}Mn_{22}N_4O_{78}$	$C_{109}H_{208}Mn_{22}Br_8N_4O_{81}$
fw (g mol^{-1})	3145.42	3931.28	4717.91
cryst syst	triclinic	orthorhombic	orthorhombic
space group	$P\bar{1}$	*Pbca*	*Pbca*
a (Å)	13.414(4)	25.229(1)	25.181(1)
b (Å)	15.906(4)	20.655(1)	20.810(1)
c (Å)	17.987(5)	33.560(1)	33.712(1)
α (deg)	66.487(2)	90	90
β (deg)	82.684(2)	90	90
γ (deg)	71.820(2)	90	90
V ($Å^3$)	3343(1)	17488(2)	17666(1)
Z	1	4	4
T (K)	150(2)	100(2)	150(2)
λ[b] (Å)	0.71073	0.71073	0.71073
D_c (g cm^{-3})	1.56	1.49	1.77
μ(Mo Kα) (mm^{-1})	1.540	1.609	3.408
measd/indep(R_{int}) reflns	61316/18776(0.047)	106948/21304(0.222)	127882/12681(0.112)
wR2[c,d]	0.1436	0.2739	0.0366
R1[d,e]	0.0457	0.0819	0.0496
GOF on F^2	0.9383	0.952	1.154

[a] Including solvate molecules. [b] Mo Kα radiation, graphite monochromator. [c] $wR2 = [\sum w(|F_o^2| - |F_c^2|)^2/\sum w|F_o^2|^2]^{1/2}$. [d] For observed data. [e] $R1 = \sum||F_o| - |F_c||/\sum|F_o|$.

$\{Mn^{II}[Mn^{II}_2Mn^{III}_4Cl_6(L^{1,5,6})_6]\}^-$ ($H_2L^{1,5,6}$ = *N*-methyl-, *N*-ethyl-, and *N*-benzyl-diethanolamine) (**d**), $\{Mn^{II}[Mn^{II}_2Mn^{III}_4Cl_3(OH)_3(hmp)_9]\}^{2+}$ (Hhmp = 2-hydroxymethylpyridine) (**e**), and $\{Mn^{II}[Mn^{II}_2Mn^{III}_4(HL^2)_3(L^2)_3]\}^{2+}$ (H_3L^2 = triethanolamine) (**f**). The second contains wheels built from simple linked "mononuclear units" often referred to as "single-stranded loops",[8a−f] examples of which include $[Mn^{III}(C_{14}H_9N_2O_3)(CH_3OH)]_{10}$ ($C_{14}H_9N_2O_3$= *N*-phenylsalicylhydrazidate) (**g**), $[Mn^{II}_6(hfac)_{12}(NITPh)_6]$ (hfac$^-$ = hexafluoroacetyl-acetonate; NITPh = 2-phenyl-4,4,5,5-tetramethyl-4,5-dihydro-*1H*-imidazolyl-1-oxyl 3-oxide) (**h**), $[Mn^{III}_6Mn^{II}_6(O_2CCH_3)_{14}(mdea)_8]$ (mdea = *N*-methyldiethanol amine) (**i**), $[Mn^{III}_4Mn^{II}_4(O_2CCH_2{}^tBu)_{12}(teaH)_4]$ ($teaH_3$ = triethanolamine) (**j**), and $[Mn^{III}_8Mn^{II}_8(O_2CCH_3)_{16}(teaH)_{12}]$ (**k**). The third category consists of wheels based on repeating polymetallic units[9] such as cubes or triangles, examples of which include $[Mn^{IV}_6Mn^{II}_{18}(bpy)_{24}(O_2CCH_3)_6(N_3)_6(tmp)_{12}]^{12+}$ (bpy = bipyridine; H_3tmp = 1,1,1-tris(hydroxymethyl)propane) (**l**) and $[Mn^{III}_{84}O_{72}(OH)_6(OCH_3)_{24}(O_2CCH_3)_{78}(CH_3OH)_{12}(H_2O)_{42}]$ (**m**). An interesting point is the similarity of the ligands/co-ligands used to generate the above complexes, the most commonly employed being carboxylates in combination with alkoxides, each bridging in a *μ*-coordination mode (though in some cases, end-on (*μ*) azides or analogous N-based ligands fulfill the role of the alkoxides). Scheme 1 shows examples (**a**−**m**) of how such ligands bridge Mn centers forming the curvature necessary for wheel formation.

Herein, we describe the syntheses, structures, and magnetic properties of three Mn wheels which belong to the third category of compounds, unusual $[Mn_{16}]$ and $[Mn_{22}]$ clusters formed from self-assembled "rod-like" and "sheetlike" moieties. We have previously published part of this work.[10] The three complexes $[Mn^{IV}_4Mn^{III}_{10}Mn^{II}_2O_2(OCH_3)_{12}(tmp)_8(O_2CCH_3)_{10}]$ (**1**), $[Mn^{IV}_2Mn^{III}_{18}Mn^{II}_2O_6(OCH_3)_{14}(O_2CCH_3)_{16}(tmp)_8(HIm)_2]$ (HIm = imidazole) (**2**), $[Mn^{IV}_2Mn^{III}_{18}Mn^{II}_2O_6(OCH_3)_{14}(O_2CCH_3)_{16}(Br-mp)_8(HIm)_2]$ (**3**) are high-spin molecules that behave as SMMs (Chart 1).

(5) See for example: (a) Aubin, S. M. J. D.; Wemple, M. W.; Maple, M. B.; Christou, G.; Hendrickson, D. N. **1998**, *120*, 839. (b) Yoo, J.; Brechin, E. K.; Yamaguchi, A.; Nakano, M.; Huffman, J. C.; Maniero, A. L.; Brunel, L. C.; Awaga, K.; Ishimoto, H.; Christou, G.; Hendrickson, D. N. *Inorg. Chem.* **2000**, *39*, 3615. (c) Koizumi, S.; Nihei, M.; Nakano, M.; Oshio, H. *Inorg. Chem.* **2005**, *44*, 1208. (d) Rajaraman, G.; Murugesu, M.; Sanudo, E. C.; Soler, M.; Wernsdorfer, W.; Helliwell, M.; Muryn, C.; Raftery, J.; Teat, S. J.; Christou, G.; Brechin, E. K. *J. Am. Chem. Soc.* **2004**, *126*, 15445.

(6) See for example: (a) McInnes, E. J. L.; Piligkos, S.; Timco G. A.; Winpenny, R. E. P. *Coord. Chem. Rev.* **2005**, *249*, 2577. (b) Laye, R. H.; McInnes, E. J. L. *Eur. J. Inorg. Chem.* **2004**, 2811. (c) Taft, K. L.; Delfs, C. D.; Papaefthymiou, G. C.; Foner, S.; Gatteschi, D.; Lippard, S. J. *J. Am. Chem. Soc.* **1994**, *116*, 823. (d) Papaefstathiou, G. S.; Manessi, A.; Raptopoulou, C. P.; Terzis, A.; Zafiropoulos, T. F. *Inorg. Chem*. **2006**, *45*, 8823. (e) King, P.; Stamatatos, T. C.; Abboud, K. A.; Christou, G. *Angew. Chem., Int. Ed*. **2006**, *45*, 7379.

(7) (a) Saalfrank, R. W.; Scheurer, A.; Prakash, R.; Heinemann, F. W.; Nakajima, T.; Hampel, F.; Leppin, R.; Pilawa, B.; Rupp, H.; Muller, P. *Inorg. Chem.* **2007**, *46*, 1586. (b) Abbati, G. L.; Cornia, A.; Fabretti, A. C.; Caneschi, A.; Gatteschi, D. *Inorg. Chem.* **1998**, *37*, 1430. (c) Koizumi, S.; Nihei, M.; Nakano, M.; Oshio, H. *Inorg. Chem.* **2005**, *44*, 1208. (d) Saalfrank, R. W.; Nakajima, T.; Mooren, N.; Scheurer, A.; Maid, H.; Hampel, F.; Trieflinger, C.; Daub, J. *Eur. J. Inorg. Chem.* **2005**, 1149. (e) Bolcar, M. A.; Aubin, S. M. J.; Folting, K.; Hendrickson, D. N.; Christou, G. *J. Chem. Soc., Chem. Commun.* **1997**, 1485. (f) Harden, N. C.; Bolcar, M. A.; Wernsdorfer, W.; Abboud, K. A.; Streib, W. E.; Christou, G. *Inorg. Chem.* **2003**, *42*, 7067. (g) Pilawa, B.; Kelemen, M. T.; Wanka, S.; Geisselmann, A.; Barra, A. L. *Europhys. Lett.* **1998**, *43*, 7.

(8) (a) Liu, S.; Lin, S.; Lin, B.; Lin, C.; Huang, J. *Angew. Chem., Int. Ed.* **2001**, *40*, 1084. (b) Caneschi, A.; Gatteschi, D.; Laugier, J.; Rey, P.; Sessoli, R.; Zanchini, C. *J. Am. Chem. Soc.* **1988**, *110*, 2795. (c) Rumberger, E. M.; Shah, S. J.; Beedle, C. C.; Zakharov, L. N.; Rheingold, A. L.; Hendrickson, D. N. *Inorg. Chem.* **2005**, *44*, 2742. (d) Rumberger, E. M.; Zakharov, L. N.; Rheingold, A. L.; Hendrickson, D. N. *Inorg. Chem.* **2004**, *43*, 6531. (e) Foguet-Albiol, D.; O'Brien, T. A.; Wernsdorfer, W.; Moulton, B.; Zaworotko, M. J.; Abboud, K. A.; Christou, G. *Angew. Chem., Int. Ed.* **2005**, *44*, 897. (f) Murugesu, M.; Wernsdorfer, W.; Abboud, K. A.; Christou, G. *Angew. Chem., Int. Ed*. **2005**, *44*, 892.

(9) (a) Scott, R. T. W.; Milios, C. J.; Vinslava, A.; Lifford, D.; Parsons, S.; Wernsdorfer, W.; Christou, G.; Brechin, E. K. *Dalton Trans.* **2006**, 3161. (b) Tasiopoulos, A. J.; Vinslava, A.; Wernsdorfer, W.; Abboud, K. A.; Christou, G. *Angew. Chem., Int. Ed*. **2004**, *43*, 2117.

(10) (a) Murugesu, M.; Wernsdorfer, W.; Raftery, J.; Christou, G.; Brechin, E. K. *Inorg. Chem.* **2004**, *43*, 4203. (b) Manoli, M.; Prescimone, A.; Mishra, K. A.; Parsons, S.; Christou, G.; Brechin, E. K. *Dalton Trans.* **2007**, *5*, 532.

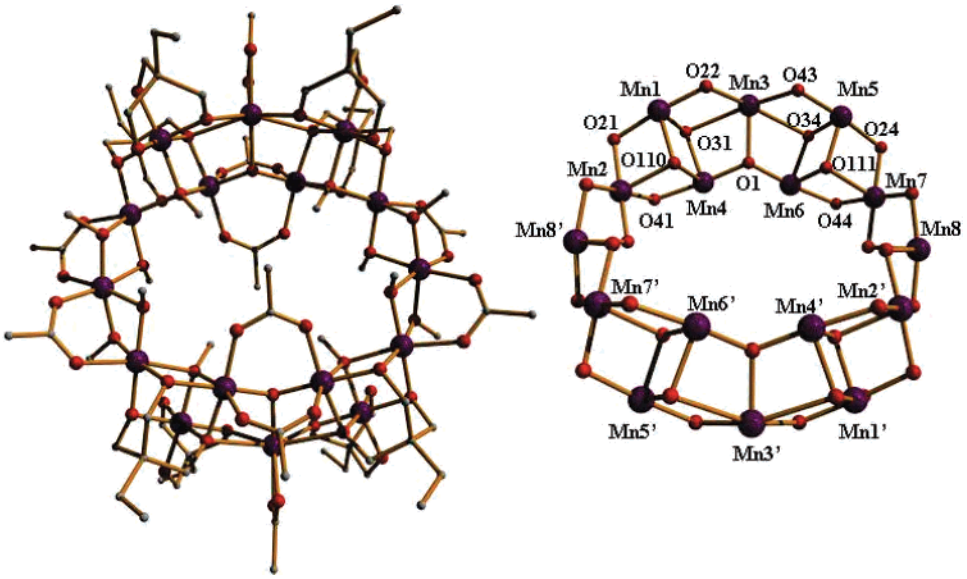

Figure 1. Molecular structure (left) and Mn−O core (right) of complex **1**. Color scheme: Mn, purple; O, red; C, gray.

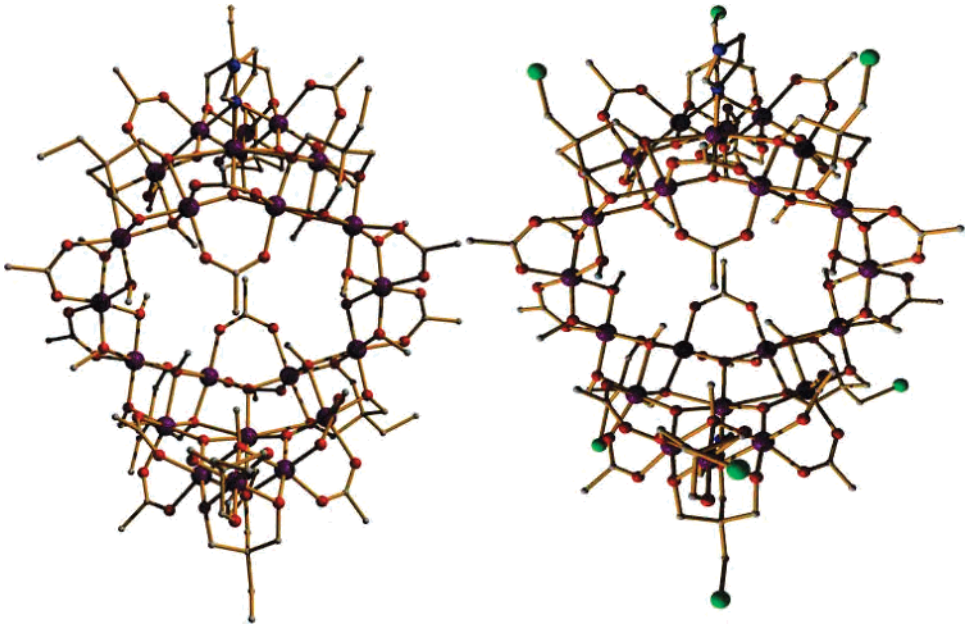

Figure 2. Molecular structures of complexes **2** (left) and **3** (right). Color scheme: Mn, purple; O, red; N, blue; C, gray; Br, green.

Experimental Section

All manipulations were performed under aerobic conditions using $[Mn_3O(O_2CCH_3)_6(HIm)_3]\cdot(O_2CCH_3)$, prepared as previously described.[11]

$[Mn^{IV}_4Mn^{III}_{10}Mn^{II}_2O_2(OCH_3)_{12}(tmp)_8(O_2CCH_3)_{10}]\cdot 3Et_2O$ (**1**·$3Et_2O$). To a stirred red-brown solution of $[Mn_3O(O_2CCH_3)_6(HIm)_3](O_2CCH_3)$ (0.500 g, 0.60 mmol) in CH_3OH (20 mL) was added solid H_3tmp (0.067 g, 0.60 mmol). The mixture was stirred for 30 min and filtered, and the resulting solution was layered with diethyl ether (Et_2O). After 7 days, black crystals of **1**·$3Et_2O$ formed and were collected by filtration, washed with Et_2O, and dried in vacuo. The yield was ∼20%. A sample for X-ray crystallography was kept in the mother liquor to prevent solvent loss. The dried complex analyzed as solvent free: Anal. Calcd (Found) for $C_{80}H_{154}Mn_{16}O_{58}$: C, 32.87 (32.44); H, 5.31 (5.00).

(11) Vincent, J. B.; Chang, H. R.; Folting, K.; Huffman, J. C.; Christou, G.; Hedrickson, D. N. *J. Am. Chem. Soc.* **1987**, *109*, 5703.

$[Mn^{IV}_2Mn^{III}_{18}Mn^{II}_2O_6(OCH_3)_{14}(O_2CCH_3)_{16}(tmp)_8(HIm)_2]\cdot 2CH_3OH$ (**2**·$2CH_3OH$). To a stirred red-brown solution of $[Mn_3O(O_2CCH_3)_6(HIm)_3](O_2CCH_3)$ (0.500 g, 0.60 mmol) in CH_3OH (20 mL) was added solid H_3tmp (0.067 g, 0.60 mmol) and $NaOCH_3$ (0.032 g, 0.60 mmol). The mixture was stirred for 12 h and filtered, and the resulting solution was layered with Et_2O. After 7 days, the resulting black crystals of **2**·$2CH_3OH$ were collected by filtration, washed with Et_2O, and dried in vacuo. The yield was ∼15%. The dried complex analyzed as solvent free: Anal. Calcd (Found) for $C_{100}H_{186}Mn_{22}O_{76}N_4$: C, 31.04 (31.21); H, 4.85 (5.13); N, 1.45 (1.78).

$[Mn^{IV}_2Mn^{III}_{18}Mn^{II}_2O_6(OCH_3)_{14}(O_2CCH_3)_{16}(Br-mp)_8(HIm)_2]\cdot 2C_6H_{14}\cdot 5CH_3OH$ (**3**·$2C_6H_{14}$·$5CH_3OH$). The synthetic procedure was similar to that followed for **2**, but with the addition of solid Br−mpH_3 (0.119 g, 0.60 mmol) instead of H_3tmp. The mixture was stirred for 40 min and then filtered, and the solution was layered with Et_2O. After 2 weeks, the resulting black crystals of **3**·$2C_6H_{14}$·$5CH_3OH$ were collected by filtration, washed with Et_2O,

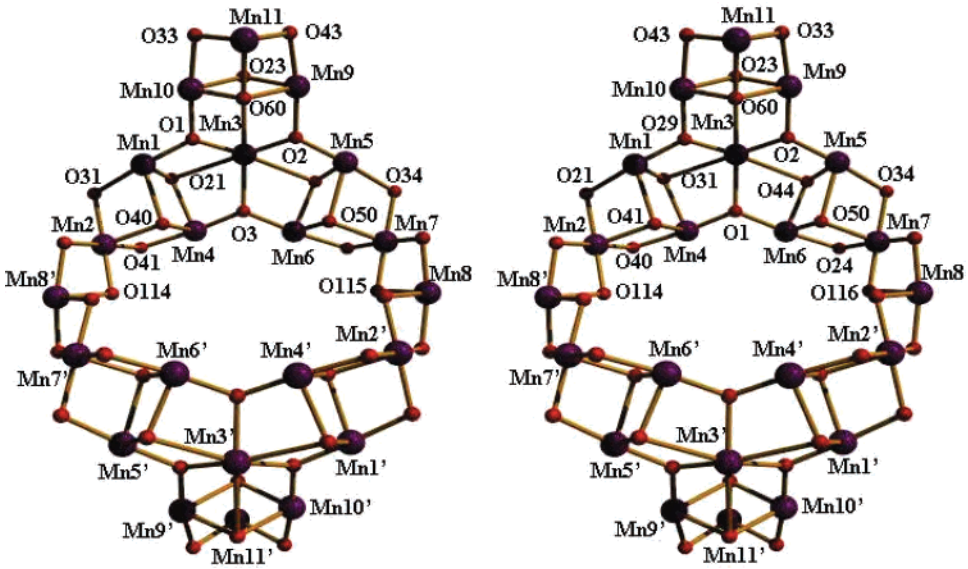

Figure 3. Mn−O cores for **2** (left) and **3** (right). Color scheme: Mn, purple; O, red.

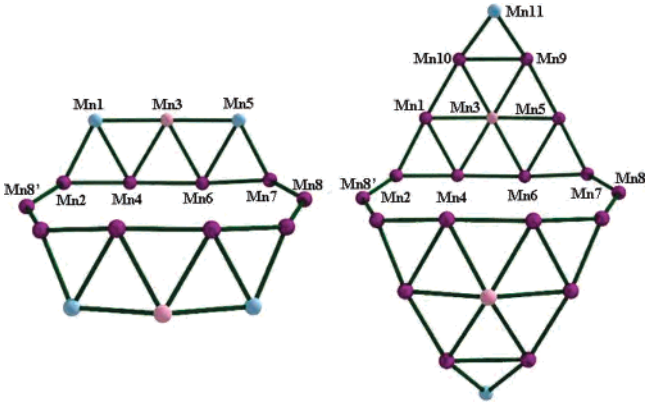

Figure 4. Metallic skeletons of complexes **1** (left) and **2** and **3** (right). Color scheme: Mn^{II}, pink; Mn^{III}, purple; Mn^{IV}, blue.

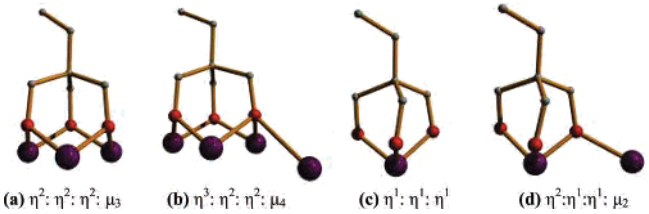

Figure 5. Coordination modes of the tripod^{3-} ligands in complexes **1**−**3**.

and dried in vacuo. The yield was ∼10%. The dried complex analyzed as solvent free: Anal. Calcd (Found) for $C_{92}H_{160}Br_8Mn_{22}O_{76}N_4$: C, 25.19 (25.09); H, 3.68 (3.46); N, 1.28 (1.47).

Physical Methods. Elemental analysis (C, H, N) were performed by the EaStCHEM microanalysis service. Variable-temperature, solid-state direct current (dc) magnetic susceptibility data down to 5 K were collected on a Quantum Design MPMS-XL SQUID magnetometer equipped with a 7 T dc magnet. Diamagnetic corrections were applied to the observed paramagnetic susceptibilities using Pascal's constants. Magnetization versus field hysteresis and dc decay measurements at temperatures below 1.8 K were performed on single crystals using a micro-SQUID instrument.[12]

X-ray Crystallography and Structure Solution. Diffraction data were collected at 150 K for **1** and **3** and at 100 K for complex **2** on a Bruker Smart Apex CCD diffractometer equipped with an Oxford Cryosystems LT device. The structures were solved by direct methods (*SHELXS*) and refined by full-matrix least-squares against F^2 (*CRYSTALS*).[13] Hydrogens were positioned geometrically and refined using the riding model. Crystallographic data and structure refinement details are listed in Table 1. Full details can be found in the accompanying CIF files.

Results and Discussion

Synthesis. Reaction of the metal triangle $[Mn^{III}_3O(O_2CCH_3)_6(HIm)_3](O_2CCH_3)$ with 1 equiv of H_3tmp in MeOH for 30 min affords the mixed-valent species **1**. If the reaction is repeated but for a period of *at least* 12 h, complex **2** forms. The same complex can be isolated in higher yields and shorter reaction times if repeated in the presence of $NaOCH_3$. If the latter reaction (including the additional $NaOCH_3$) is repeated with 2-(bromomethyl)-2-(hydroxymethyl)-1,3-propanediol (Br−mpH_3) with stirring for 40 min, the complex **3** forms. It is difficult to speculate on the reaction pathways that lead to the formation of the three complexes—as is the case with all Mn cluster chemistry—but it has been shown previously that μ_5-bridging (the most commonly observed coordination mode for these ligands) fully deprotonated tripodal alcohols favor the formation of one-dimensional rod-like complexes in Mn carboxylate chemistry.[4d] Additionally, the use of alcohol as solvent and the consequent presence of μ-bridging CH_3O^- ions may also favor the formation of the inner Mn^{III}_{10} wheel (vide infra). Decametallic wheels of general formula $[M^{III}_{10}(OR)_{20}(O_2CR)_{10}]$ (R = Me, Et, etc.) are well-known for Fe^{III}, Ga^{III}, Cr^{III}, and V^{III} and can be made easily from the reaction of the appropriate M^{III} triangle $([M^{III}_3O(O_2CR)_6L_3]^+$ (L = H_2O, CH_3OH, etc.) with alcohol.[6] These complexes describe a near-planar circular array of M^{III} ions in which each pair of metal ions is bridged

(12) Wernsdorfer, W. *Adv. Chem. Phys.* **2001**, *118*, 99.

(13) Betteridge, P. W.; Carruthers, J. R.; Cooper, R. I.; Prout, K.; Watkin, D. J. *J. Appl. Crystallogr.* **2003**, *36*, 1487.

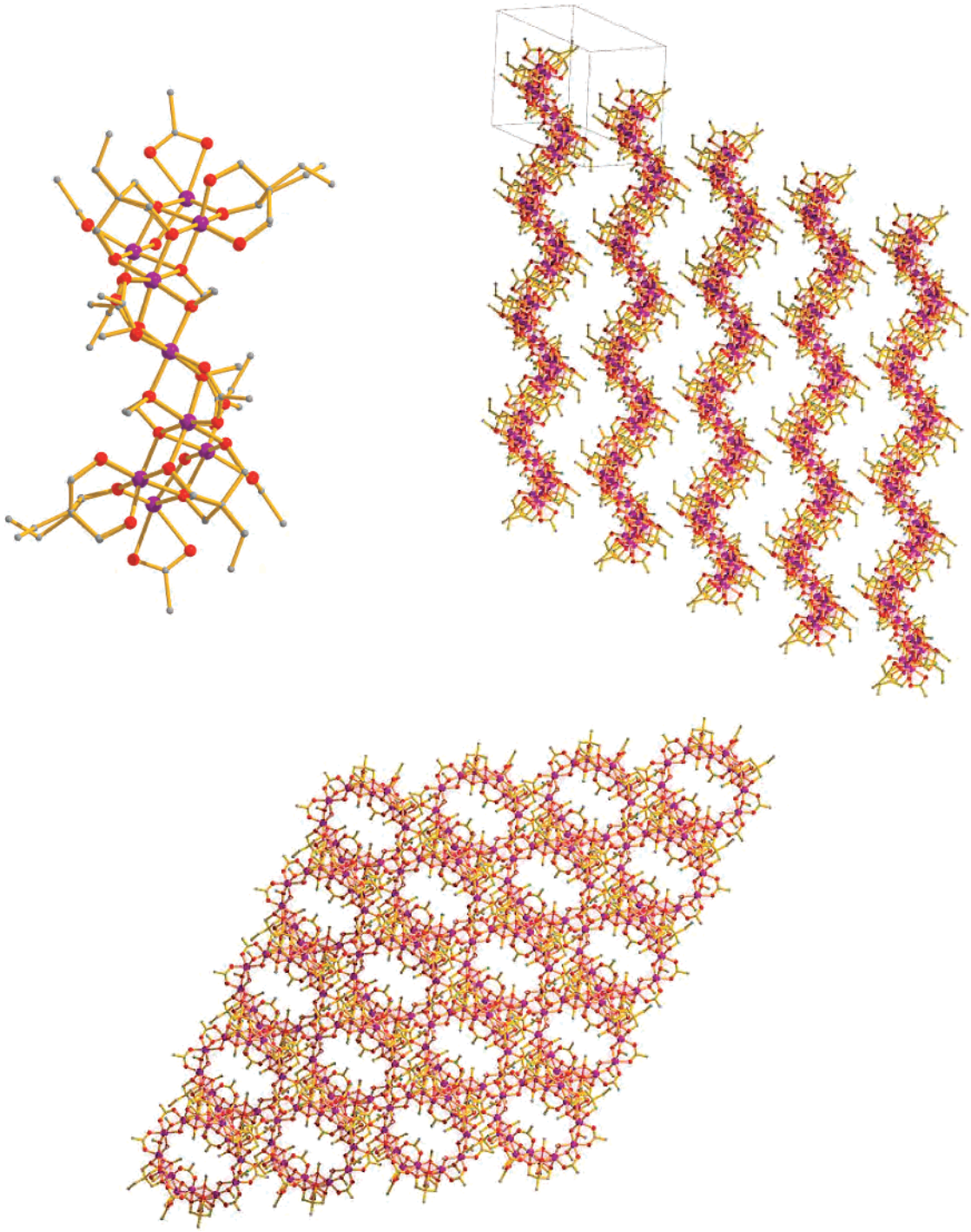

Figure 6. Side view (i.e., parallel to the Mn_{10} inner wheel) of complex **1** highlighting its S shape (top left). The packing of molecules of **1** in the crystal, highlighting the serpentine-like chains (top right), and the "figures-of-eight" chains (bottom), viewed parallel and perpendicular to the Mn_{10} inner wheels, respectively.

by two μ-alkoxides and one μ-carboxylate. The central $[Mn^{III}_{10}O_2(OR)_{16}(O_2CR)_8]$ core displayed by **1**−**3** is remarkably similar (Scheme 2), perhaps suggesting that the initial step in the syntheses is the formation of a decametallic Mn^{III} wheel, to which further metal ions are added as a result of the presence of additional bridging (tripodal) alkoxides. This in turn suggests that the Mn^{III} analogue of $[M^{III}_{10}(OR)_{20}(O_2CR)_{10}]$ can be made by simply reacting $[Mn^{III}_3O(O_2CR)_6L_3]^+$ species with alcohol. This is currently under investigation.

Description of Structures. Complex **1** crystallizes in the triclinic space group $P\bar{1}$ (Figure 1; selected bond lengths and angles are given in Supporting Information Tables SI1 and SI2, respectively). The core of **1** (Figure 1) consists of a central near-planar $[Mn^{III}_{10}]$ single-stranded loop (containing Mn2, Mn4, Mn6, Mn7, Mn8, and symmetry equivalents, s.e.) to which six further Mn ions are attached (Mn1, Mn3, Mn5, and s.e.), three above and three below opposite "sides" of the Mn_{10} wheel. The metallic skeleton of complex **1** (Figure 4) thus describes two offset stacked parallel $[Mn_7]$ "rods"

Scheme 2. The Central Mn^{III}_{10} Wheel Present in **1**−**3** (left) and Its Comparison to the Decametallic Wheels of General Formula $[M^{III}_{10}(OR)_{20}(O_2CR)_{10}]$ (right)

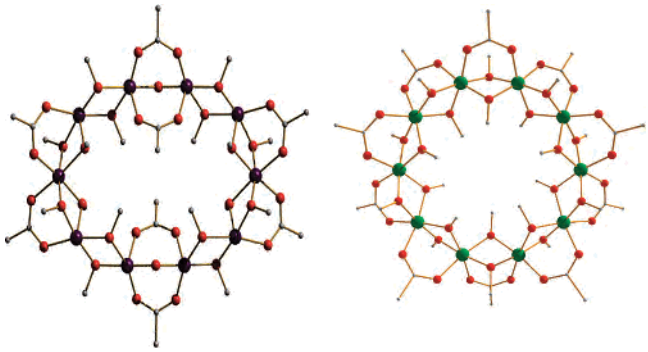

(containing Mn1−Mn7 and comprising five edge-sharing triangles) linked by two apical Mn ions (Mn8 and s.e.) into a loop. Each "half" of the $[Mn_{16}O_{30}]^{10-}$ metal−oxygen core (Figure 3) describes two $[Mn_3O_4]$ partial cubes (Mn1, Mn2, Mn4; Mn5−Mn7) linked to a central $[Mn_3O]$ triangle (Mn3, Mn4, Mn6, O1) via the oxygen atoms of one η^1:η^1:η^2:μ_2-tmp^{3-}, one η^2:η^2:η^2:μ_3-tmp^{3-}, one μ_3-OCH_3^-, and one μ-$O_2CCH_3^-$ ligand, with the two halves then linked at the apical Mn sites via a combination of two μ-OCH_3^- and two μ-$O_2CCH_3^-$ ligands. The oxygen atoms of the $[Mn_3O_4]$ partial cubes are derived from two η^2:η^2:η^2:μ_3-tmp^{3-} ligands (O21−O31−O41 and O24−O34−O44), two μ_3-OCH_3^- (O110 and O111) ligands, and those of the $[Mn_3O]$ triangles from the sole O^{2-} ions (O1 and s.e.).

Complexes **2** and **3** (Figures 2 and 3; selected bond lengths and angles are given in Supporting Information Tables SI3−SI6) crystallize in the orthorhombic space group *Pbca*. Remarkably, the same $[Mn_{16}O_{30}]^{10-}$ metal−oxygen core (Figure 3) is maintained, with two additional $[Mn_3O_4]$ partial cubanes (Mn9−Mn11 and s.e.) attached via the oxygen atoms of one η^2:η^2:η^2:μ_3-Br−mp^{3-} ligand (O23, O33, O43), one μ-OCH_3^- ligand (O60), and four μ-$O_2CCH_3^-$ ligands on each side (one above and one below) the two "Mn_7 rods". Thus, the metallic skeletons of **2** and **3** (Figure 4) describe two offset Mn_{10} "triangular sheets" (containing Mn1−Mn11 and s.e.) comprising nine edge-sharing triangles linked by two apical Mn^{III} ions (Mn8 and s.e) into a loop.

The tripodal alcohol ligands in complexes **1**−**3** are all triply deprotonated ($tripod^{3-}$) and bridge in two different modes for complex **1** and three different modes for **2** and **3**; these are shown in Figure 5. In **1**, four adopt the η^2:η^2:η^2:μ_3-mode (Figure 5a) and four adopt the η^2:η^1:η^1:μ_2-mode (5d). In **2** and **3**, two coordinate in a η^2:η^2:η^2:μ_3-fashion (Figure 5a), four coordinate in a η^3:η^2:η^2:μ_4-fashion (Figure 5b), and two chelate (Figure 5c), bonding only to Mn11 (and s.e.). The CH_3O^- ligands adopt two coordination modes, a μ_3-mode, each forming a corner of the $[Mn_3O_4]$ partial cubes (thus appearing four times in **1** and six times in **2** and **3**), and the simple μ-mode, bridging Mn_2 pairs. For **1**, all the CH_3O^- ligands are found bridging within the central Mn_{10} wheel. For **2** and **3**, the one "additional" μ_3-methoxide resides in the peripheral $[Mn_3O_4]$ partial cube. The $CH_3CO_2^-$ ligands in **2** and **3** all bond in the expected μ-mode (with the two HIm ligands bonding terminally to the tetrahedral Mn^{II} ions), but in complex **1**, one acetate (and s.e) adopts the more unusual chelating mode, bonding only to the five-coordinate Mn^{II} ion. The cavities within the central Mn_{10} wheels are oval-shaped, with metal−metal distances of Mn8−Mn8′ equal to 11.15 Å (**1**), 10.99 Å (**2**), and 10.93 Å (**3**) and metal−metal distances of Mn4−Mn6′ equal to 8.07 Å (**1**), 8.37 Å (**2**), and 8.47 Å (**3**). All oxidation states were assigned using a combination of bond lengths, charge balance considerations, and bond valence sum calculations (Supporting Information Table SI7).[14]

Despite their obvious similarities, there are some differences between the two classes of complexes (**1** vs **2** and **3**), particularly regarding the observed oxidation level (Figure 4 and Supporting Information Table SI7) and the geometry of the Mn centers. For **1**, the Mn ions in the single-stranded central Mn_{10} wheel are all six-coordinate Mn^{III} ions in Jahn−Teller distorted-octahedral geometries. Mn3 (and s.e.) is a five-coordinate Mn^{II} ion in distorted-trigonal-bipyramidal geometry, and Mn1 and Mn5 (and s.e.) are six-coordinate Mn^{IV} ions in slightly distorted-octahedral geometries. For **2** and **3**, the Mn ions in the single-stranded central Mn_{10} wheel are again all six-coordinate Mn^{III} ions in Jahn−Teller distorted-octahedral geometries. Mn3 (and s.e.) is a four-coordinate Mn^{II} ion in tetrahedral geometry, and Mn11 (and s.e.) is a six-coordinate Mn^{IV} ion.

Figures 6 and 7 show the packing diagrams of complexes **1** and **2**/**3**, respectively. Complex **1** crystallizes in the triclinic space group $P\bar{1}$ and contains two half $[Mn_{16}]$ molecules in the unit cell such that the clusters are oriented in the same direction throughout the crystal. There are no intermolecular H-bonds (see the CIF in the Supporting Information for details of disordered Et_2O), with the shortest intermolecular interactions of ∼3.3 Å between the methyl group of an acetate on one molecule and an O atom of an acetate ligand on its neighbor. Complexes **2** and **3** crystallize in orthorhombic space group *Pbca* and contain four $[Mn_{22}]$ molecules per unit cell, oriented in two different directions. Here, the intermolecular H-bonds are extensive: the O arms of the terminally bound $tripod^{3-}$ ligands H-bond to either a CH_3OH solvate molecule (e.g., O5−O39, 2.860 Å) or an imidazole on a neighboring molecule; the protonated N atom of the HIm ligands H-bonds to $CH_3CO_2^-$ ligands on neighboring molecules (e.g., N2−O4, 2.882 Å; N2−O7, 2.925 Å), as do the MeOH solvent molecules. The closest distance between individual $[Mn_{22}]$ molecules occurs between the protonated N atom of the HIm ligand and the O atoms of the $tripod^{3-}$ ligand (e.g., N2−O22, 2.935 Å). For all three compounds, the clusters pack in a "head-to-tail" fashion, forming an overall serpentine-like or zigzag packing of the molecules in the crystal. For **2** and **3**, the peripherally attached $[Mn_3O_4]$ partial cubes enhance the S shape of the individual $[Mn_{22}]$ clusters with respect to the $[Mn_{16}]$ molecule, making this packing motif even more pronounced (Figure 7).

Magnetic Studies. Direct current magnetic susceptibility measurements (χ_M) were performed on powdered crystalline

(14) Thorp, H. H. *Inorg. Chem.* **1992**, *31*, 1585.

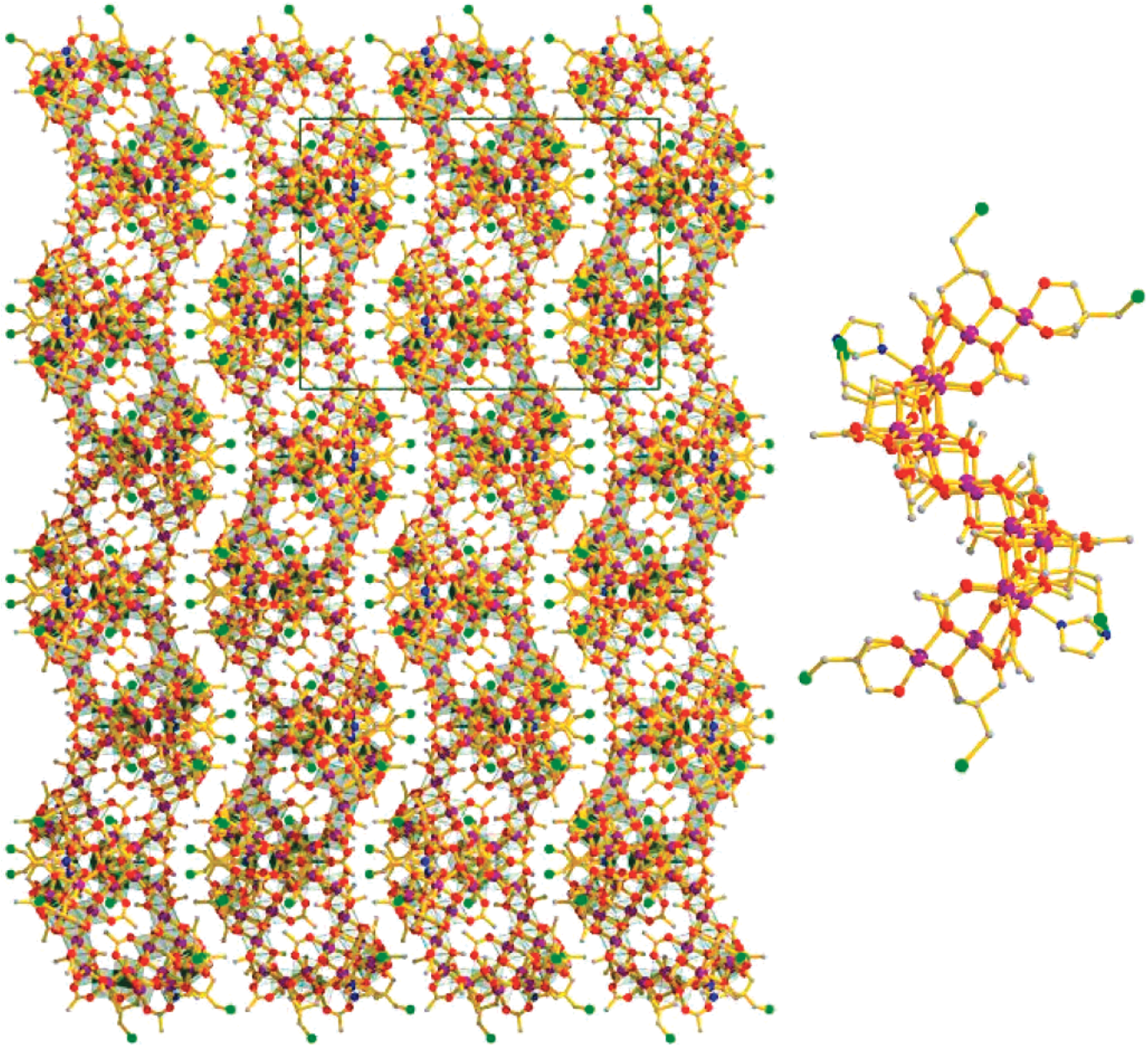

Figure 7. Side-view (i.e., parallel to the Mn_{10} inner wheel) of complex **3** highlighting its S shape (right) and the packing of molecules of **3** in the crystal highlighting the serpentine-like chains (left).

samples of **1**−**3** in the temperature range of 5−300 K under an applied field of 0.1 T. These are plotted as $\chi_M T$ vs T in Figure 8. For complex **1**, the $\chi_M T$ value at 300 K of 47.4 $cm^3\ mol^{-1}\ K$ is higher than the spin-only ($g = 2$) value of 46.3 $cm^3\ mol^{-1}\ K$ expected for 2 Mn^{II}, 10 Mn^{III}, and 4 Mn^{IV} ions. Upon cooling, the $\chi_M T$ value increases slightly to a value of 51.4 $cm^3\ mol^{-1}\ K$ at 50 K, then increases rapidly and reaches a maximum value of 88.4 $cm^3\ mol^{-1}\ K$ at 6.5 K before falling to 87.9 $cm^3\ mol^{-1}\ K$ at 5 K. The low-temperature (maximum) $\chi_M T$ value suggests a spin ground-state value of $S = 14 \pm 1$ (88.4 $cm^3\ K\ mol^{-1}$).

The room-temperature $\chi_M T$ value for complex **2** is ∼56 $cm^3\ mol^{-1}\ K$, lower than the expected spin-only value of 66.5 $cm^3\ mol^{-1}\ K$ expected for 2 Mn^{IV}, 18 Mn^{III}, and 2 Mn^{II} ions. The $\chi_M T$ value decreases steadily upon cooling to 48.3 $cm^3\ K\ mol^{-1}$ at 30 K and then slightly increases to reach a maximum value of 48.6 $cm^3\ mol^{-1}\ K$ at 15 K before dropping rapidly to 40.3 $cm^3\ mol^{-1}\ K$ at 5 K. The 15 K $\chi_M T$ value indicates an approximately $S = 10 \pm 1$ (48.6 $cm^3\ mol^{-1}$ K) spin ground-state value. For complex **3**, the $\chi_M T$ value at 300 K is ∼62.5 $cm^3\ mol^{-1}\ K$. Upon cooling, it decreases steadily to ∼52.5 $cm^3\ mol^{-1}\ K$ at 50 K, before increasing to reach a maximum value of ∼57 $cm^3\ mol^{-1}\ K$ at 15 K and then dropping rapidly to 52 $cm^3\ mol^{-1}\ K$ at 5 K. The low-temperature maximum is suggestive of $S = 10 \pm 1$. The decreases in $\chi_M T$ values at low temperature are likely a consequence of Zeeman effects from the dc field, zero-field splitting, and/or the presence of intermolecular antiferromagnetic interactions.

Magnetization measurements in the respective 1.8 to 10 K and 0.1 to 7 T temperature and magnetic-field ranges were carried out to determine the spin ground-state values for **1**−**3**. The data were fit by a matrix-diagonalization method to a model that assumes only the ground state is populated,

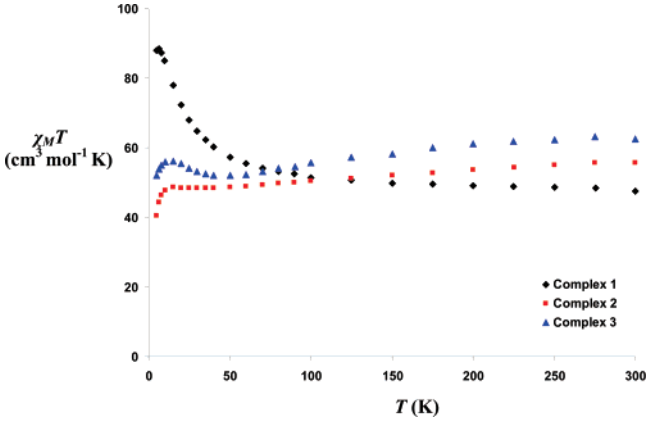

Figure 8. Plot of $\chi_M T$ vs T for complexes **1**−**3** in the 5−300 K temperature range in a field of 0.1 T.

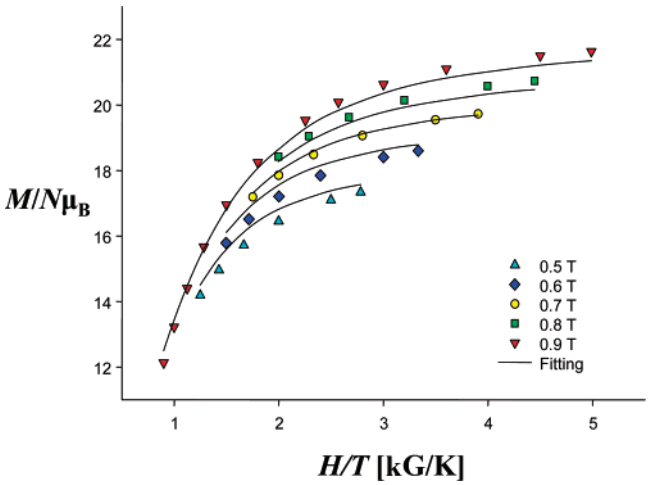

Figure 9. Plot of reduced magnetization ($M/N\mu_B$) vs H/T for **1**. The solid lines are the fit of the data to an $S = 14$ state with $D = -0.040$ cm^{-1} and $g = 1.85$.

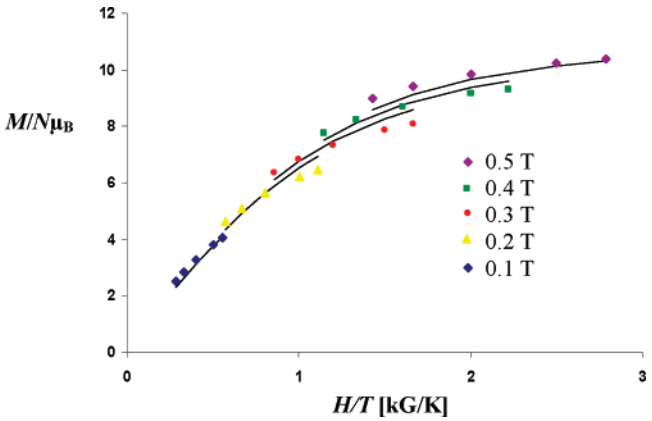

Figure 10. Plot of reduced magnetization ($M/N\mu_B$) vs H/T for **3**. The solid lines are the fit of the data to an $S = 9$ state with $D = -0.165$ cm^{-1} and $g = 2.00$.

includes axial zero-field splitting ($D\hat{S}_z^2$), and carries out a full powder average. The corresponding Hamiltonian is

$$\hat{H} = D\hat{S}_z^{\,2} + g\mu_B\mu_0\,\hat{S}\cdot H$$

where D is the axial anisotropy, μ_B is the Bohr magneton, μ_0 is the vacuum permeability, $\hat{S}_z$ is the easy-axis spin operator, and H is the applied field. The data is plotted as

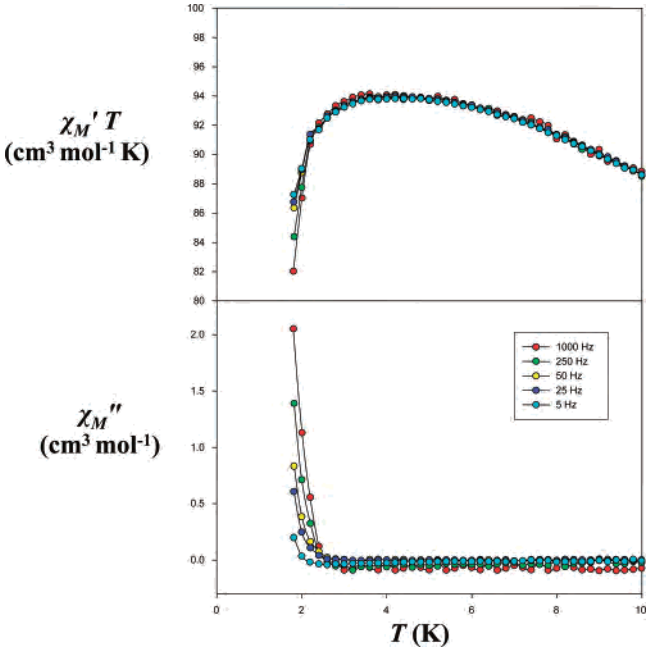

Figure 11. Plot of the in-phase (as $\chi'_M T$) (top) and out-of-phase (χ''_M) ac susceptibility signal (bottom) vs temperature for complex **1**.

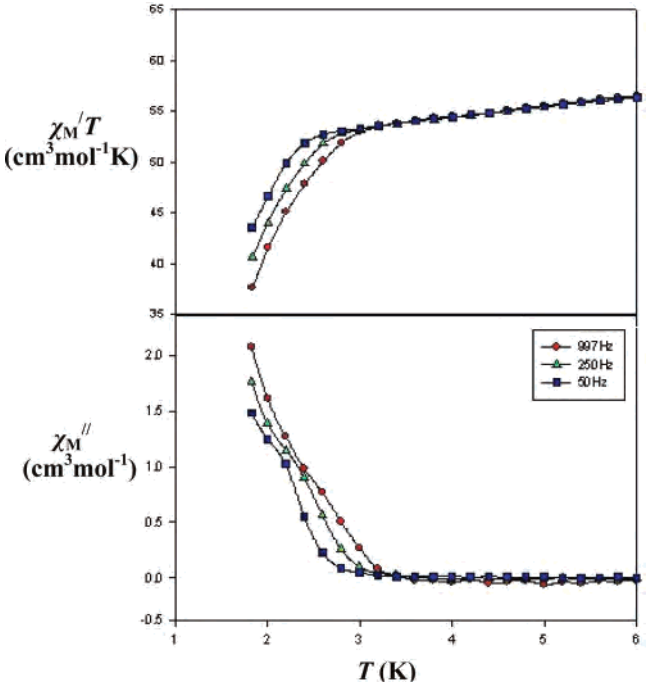

Figure 12. Plots of the in-phase (as $\chi'_M T$) (top) and out-of-phase (χ''_M) (bottom) ac susceptibility signal vs temperature for complex **3**.

reduced magnetization ($M/N\mu_B$) versus H/T in Figures 9 and 10. The best fit for complex **1** gave $S = 14$, $g = 1.85$, and $D = -0.04$ cm^{-1} using only low field (≤ 1 T) data. When fields up to 7 T were employed, poorer quality fits were obtained. This behavior is characteristic of the presence of low-lying excited states. In such cases, the population of the excited states is difficult to avoid—even at very low temperatures. Because the fitting procedure assumes that only the ground state is populated at low temperatures, the use of data collected at higher fields tends to overestimate the value of S, and consequently, the use of only low-field data

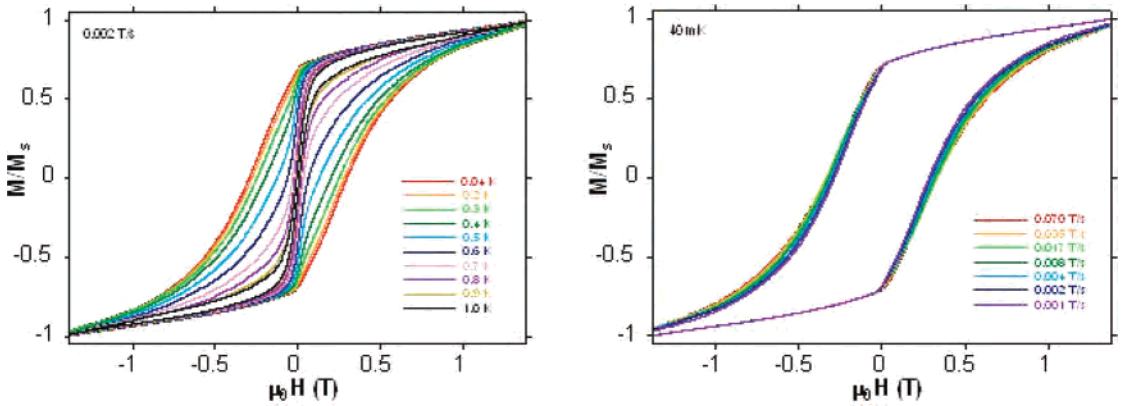

Figure 13. Magnetization (M) vs dc field hysteresis loops for **1**, at a field scan rate of 0.002 T/s in the temperature range of 1.0−0.04 K (left) and at a temperature of 0.04 K in the field sweep rate range of 0.07−0.001 T/s (right). M is normalized to its saturation value.

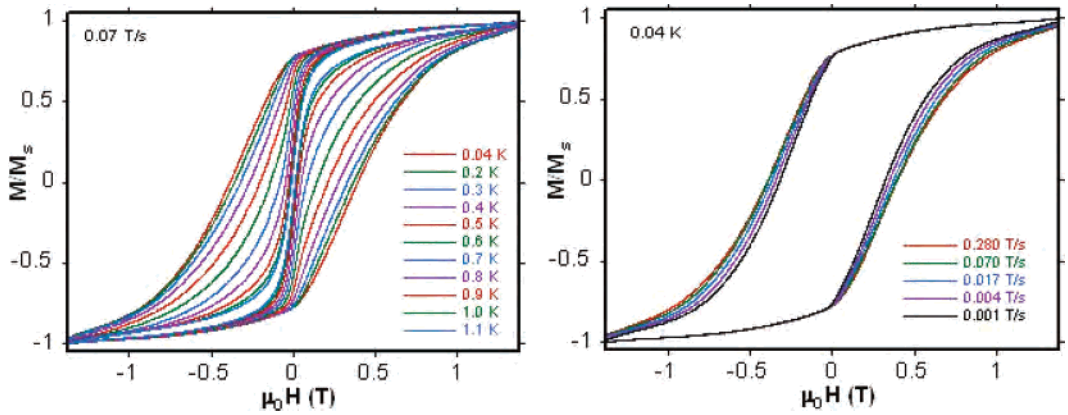

Figure 14. Magnetization (M) vs dc field hysteresis loops for **2,** at a field scan rate of 0.07 T/s in the temperature range of 1.1−0.04 K (left) and at a temperature of 0.04 K in the field scan rate range of 0.280−0.001 T/s (right). M is normalized to its saturation value.

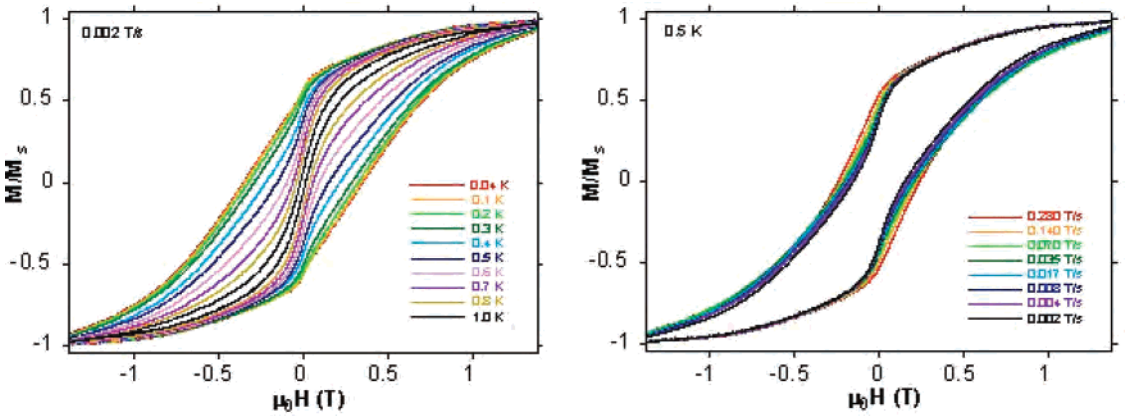

Figure 15. Magnetization (M) vs dc field hysteresis loops for **3,** at a field scan rate of 0.002 T/s in the temperature range of 1.0−0.04 K (left) and at a temperature of 0.5 K in the field scan rate range of 0.280−0.002 T/s (right). M is normalized to its saturation value.

in the fits helps to avoid this problem, providing more reliable results. For example, for complex **1**, the value of $M/N\mu_B$ rises to approximately 36 in a field of 7 T, suggestive of $S = 18$. However, this is not the true ground-state value, and attempts to fit the magnetization data with $S = 18$ resulted in much poorer quality fits with unreasonable parameters (D and g). The magnitude of $|D|$ is consistent with the nonparallel allignment of the Jahn−Teller axes of the Mn^{III} ions. The best fit for complex **2** was $S = 9$, $g = 2.00$, and $D = -0.129$ cm^{-1}, and for complex **3** the best fit was $S = 9$, $g = 2.00$, and $D = -0.165$ cm^{-1}, both using data collected in the field range of 0.1−0.5 T. The S and D values obtained for complexes **1**−**3** suggest that all three may exhibit single-molecule magnetism behavior.

In-phase (χ'_M) and out-of-phase (χ''_M) alternating current (ac) susceptibility measurements were performed on complexes **1**−**3** in the 1.8−10 K range in a 3.5 G ac field oscillating at 5−1000 Hz. For complex **1** (Figure 11), there is first an increase in the value of $\chi'_M T$ with decreasing temperature to approximately 6 K, followed by a plateau until ∼3 K, suggesting the presence of low-lying excited states with smaller S values. Such low-lying excited states are a common feature in many Mn clusters that are of either high nuclearity and thus possess a large density of spin states

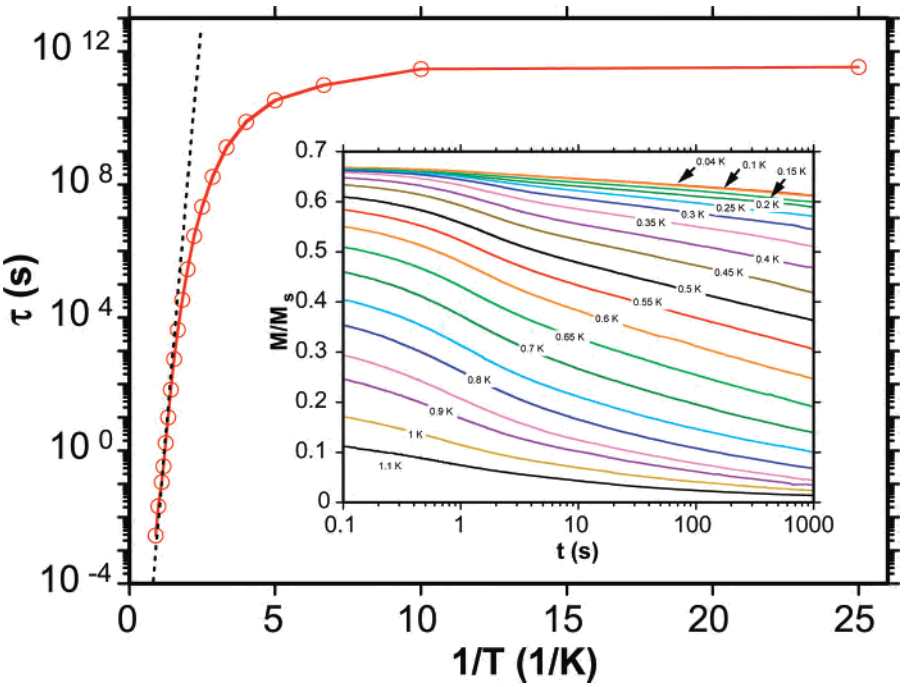

Figure 16. Arrhenius plot for **1** using dc relaxation data (inset). The dashed line is the fit of the thermally activated region to the Arrhenius equation.

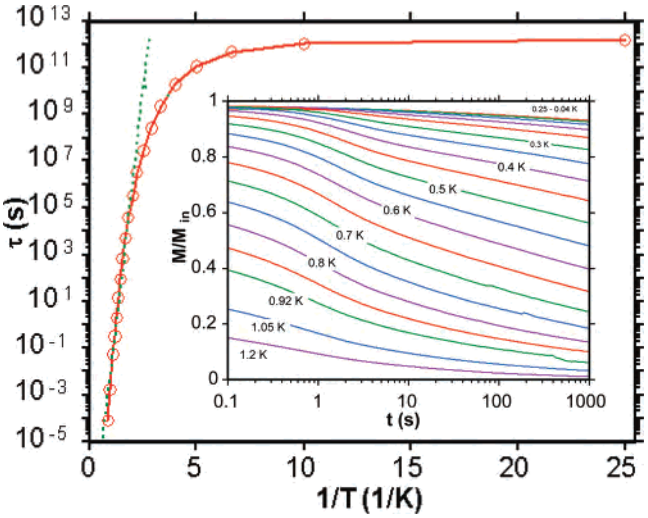

Figure 17. Arrhenius plot for **2** using dc relaxation data (inset). The dashed line is the fit of the thermally activated region to the Arrhenius equation.

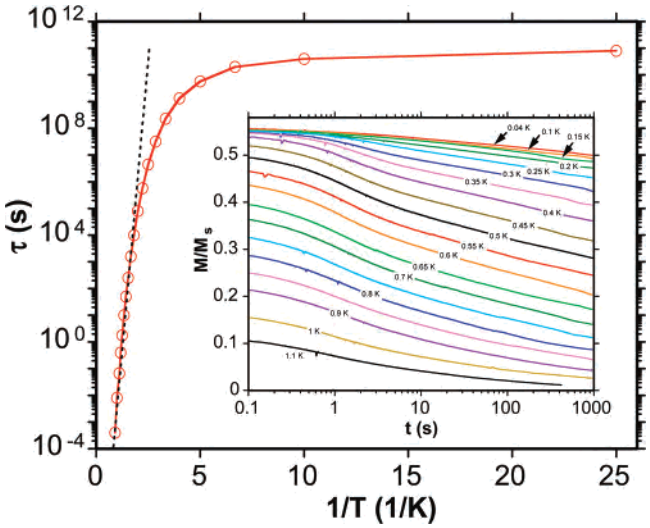

Figure 18. Arrhenius plot for **3** using dc relaxation data (inset). The dashed line is the fit of the thermally activated region to the Arrhenius equation.

or contain multiple Mn^{II} ions that typically promote weak exchange. Extrapolation to 0 K (from >3 K to avoid decreases due to effects such as intermolecular interactions, etc.) gives a value of ~94 cm^3 mol^{-1} K, consistent with a spin ground-state value of $S = 14$, in agreement with the dc data. Frequency-dependent out-of-phase χ''_M ac susceptibility signals are seen for below approximately 2.5 K (Figure 11), but no peaks are observed.

The behavior of **2** and **3** is similar: below 10 K, both show sloping lines with a slight decrease in $\chi'_M T$ with decreasing temperature, suggesting the presence of excited states with larger S values (Figure 12). Extrapolation of the slopes to 0 K gives values of ~53 cm^3 mol^{-1} K for both, suggesting spin ground-state values of $S = 10 \pm 1$, in agreement with the dc data. Frequency-dependent out-of-phase (χ''_M) ac susceptibility signals are seen for both complexes below approximately 3 K, but no peaks are observed, along with a concomitant decrease in the in-phase signal. The presence out-of-phase signals is suggestive of single-molecule magnetism behavior and is caused by the inability of **1**−**3** to relax quickly enough, at these temperatures, to keep up with the oscillating field.

In order to probe the possible single-molecule magnetism behavior, single-crystal hysteresis loop and relaxation measurements were performed using a micro-SQUID setup.[12] Studies of the magnetization performed at very low temperature and high fields show that all three complexes behave as SMMs with long relaxation times. Figures 13−15 present typical magnetization (M) vs applied dc field measurements at different field sweep rates and temperatures. In each case, hysteresis loops were observed, whose coercivities increase with decreasing temperature or increasing field sweep rate,

as expected for the superparamagnetic-like behavior of a SMM. Above ~1.3 K, there is no hysteresis; i.e., the spin relaxes faster to equilibrium than the time scale of the hysteresis loop measurement. The hysteresis loops do not show the steplike features indicative of resonant quantum tunneling of magnetization between the energy states of the molecule. This absence is commonplace for large SMMs and can be rationalized as primarily due to a distribution of molecular environments and thus a distribution of magnetization relaxation barriers. Weak intermolecular interactions (exchange and/or dipolar) and low-lying excited states will also contribute to step broadening.[15]

Single-crystal relaxation data collected for **1**−**3** with the field applied along the easy axis of magnetization are shown in Figures 16−18. The observed nonexponential relaxations and Arrhenius plots are typical for such large molecules with rather weak anisotropy and low-lying excited spin states. It is clear that the giant spin approximation works badly for such molecules (i.e., the ground-state spin is not well-defined) and that the slow relaxation is due to relaxation between different spin states, as well as between up and down states of a given multiplet. The relaxations are also influenced by intermolecular interactions and the distribution of molecular environments, leading to a broad distribution of relaxation times. Despite these difficulties (and by employing a single scaling function $f(t/\tau(T)$[16]) we could extract the mean relaxation times $\tau(T)$ for all three complexes, which are shown in Figures 16−18 in the form of Arrhenius plots. The straight lines are fits to the Arrhenius law, yielding the values $\tau_0 = 9 \times 10^{-11}$ s and $U_{\text{eff}} = 19$ K for **1**, $\tau_0 = 3 \times 10^{-11}$ s and $U_{\text{eff}} = 19$ K for **2**, and $\tau_0 = 2 \times 10^{-11}$ s and $U_{\text{eff}} = 19.8$ K for **3**.

(15) See for example: (a) Sañudo, E. C.; Brechin, E. K.; Boskovic, C.; Wernsdorfer, W.; Yoo, J.; Yamaguchi, A.; Concolino, T. R.; Abboud, K. A.; Rheingold, A. L.; Ishimoto, H.; Hendrickson, D. N.; Christou, G. *Polyhedron* **2003**, *23*, 2267. (b) Jones, L. F.; Brechin, E. K.; Collison, D.; Harrison, A.; Teat, S. J.; Wernsdorfer, W. *Chem. Commun*. **2002**, 2974. (c) Soler, M.; Rumberger, E.; Folting, K.; Hendrickson, D. N.; Christou, G. *Polyhedron* **2001**, *20*, 1365. (d) Soler, M.; Wernsdorfer, W.; Folting, K.; Pink, M.; Christou, G. *J. Am. Chem. Soc*. **2004**, *126*, 2156.

(16) (a) Thomas, L.; Caneschi, A.; Barbara, B. *Phys. Rev. Lett*. **1999**, *83*, 2398. (b) Affronte, M.; Lasjaunias, J. C.; Wernsdorfer, W.; Sessoli, R.; Gatteschi, D.; Heath, S. L.; Fort, A.; Rettori, A. *Phys. Rev. B: Condens. Matter Mater. Phys.* **2002**, *66*, 064408.

Conclusions

In conclusion, we have synthesized rare examples of high-nuclearity, high-spin Mn wheels. The complexes were isolated from the same reaction but in different time scales and/or with different tripodal alcohols, demonstrating the versatility of a simple reaction system. All three structures are near-identical, with the differences limited to the oxidation levels of the Mn ions and the presence of two additionally attached $[Mn_3O_4]$ partial cubes in the Mn_{22} complexes. In each case, their synthesis *may* be governed by the initial formation of a decametallic inner wheel with the tripodal alcohols then directing the formation of edge-sharing triangular moieties that are attached to either side of the Mn_{10} wheel. The alcohol-induced formation of M^{III}_{10} wheels is well-known for Fe, Ga, Cr, and V, suggesting that the Mn analogue may be isolable from the simple reaction of $[M^{III}_3O(O_2CR)_6L_3]^+$ with alcohol. Complexes **1**−**3** are among the largest nuclearity and highest-spin Mn SMMs known—indeed, the $S = 14$ ground-state value displayed by **1** is the largest seen for any Mn wheel.

Supporting Information Available: CIF files, tables of interatomic distances and angles, and BVS calculations for **1**−**3**. This material is available free of charge via the Internet at http://pubs.acs.org.

IC7007528